Use of dynamic schlieren interferometry to study fluctuations during free diffusion

Fabrizio Croccolo, Doriano Brogioli, Alberto Vailati, Marzio Giglio, and David S. Cannell

We used a form of schlieren interferometry to measure the mean-squared amplitude and temporal autocorrelation function of concentration fluctuations driven by the presence of a gradient during the free diffusion of a urea solution into water. By taking and processing sequences of images separated in time by less than the shortest correlation time of interest, we were able to simultaneously measure dynamics at a number of different wave vectors. The technique is conceptually similar to the shadowgraph method, which has been used to make similar measurements, but the schlieren method has the advantage that the transfer function is wave-vector independent rather than oscillatory.

OCIS codes: 030.6600, 070.2580, 070.6760, 110.4850, 290.5820.

1. Introduction

A. Classical Scattering Methods

Since the invention of the laser, dynamic light scattering (DLS) has been used to study the dynamics of a wide variety of phenomena, including density fluctuations in liquids and gases; Brownian motion of colloidal particles; diffusion in protein, polymer, and polyelectrolyte solutions; critical dynamics of single-component fluids and mixtures; aggregation and flocculation processes; etc.[1] Its popularity stems from the fact that the technique is accurate and noninvasive, provides absolute results, and covers a wide range of correlation times. Traditional DLS relies on measuring fluctuations in the intensity of the scattered light in the far field, free of any significant contribution from the beam or from stray elastically scattered light, which originates from every optical surface involved (homodyne detection). In practice, this requirement usually limits the classical homodyne method to scattering angles of several degrees or more, i.e., to the study of fluctuations having wavelengths of the order of micrometers or shorter. Alternatively, stray light or a portion of the original beam, which is much more intense than the scattered light, can be deliberately mixed with the scattered light (heterodyne method), although this is not so common in practice. Samples that scatter very weakly may be measured accurately, which is one of the strengths of the method.

More recently, light-scattering instruments were described in which the traditional single sensor (usually a photomultiplier tube) was replaced by a pixilated sensor, such as a CCD camera.[2–4] In this way it is possible to measure scattering at a large number of independent scattering wave vectors simultaneously, and this can greatly improve the precision obtainable at a given time. The use of such a method for DLS seems to have been pioneered by Wong and Wiltzius[2] and then extended to very low scattering angles by Cipelletti and Weitz,[3] who utilized an optical scheme very similar to that described by Ferri[4] for low-angle elastic light scattering. In all of these schemes some method is present to remove the beam and allow the scattered light alone to fall on the sensor. Of course, the fluctuations responsible for the scattering must be relatively slow and the scattering must be relatively strong to use such sensors.

B. Alternative Scattering Methods

Alternative scattering techniques, in which no attempt is made to separate the scattered light from the transmitted beam and which allow measurement of both the amplitude and the dynamics of long-wavelength fluctuations, have recently begun to

F. Croccolo, D. Brogioli, A. Vailati (vailati@fisica.unimi.it), and M. Giglio are with CNR–Istituto Nationale per la Fisica della Materia (INFM) and Dipartimento di Fisica, Università degli Studi di Milano, Via Celoria 16, 20133 Milan, Italy. D. S. Cannell is with the Department of Physics and iQCD, University of California, Santa Barbara, Santa Barbara, California 93106.

Received 15 August 2005; accepted 22 September 2005; posted 1 December 2005 (Doc. ID 64083).

0003-6935/06/102166-08$15.00/0

emerge.[5–12] We are aware of three such methods: namely, the quantitative shadowgraph,[12] heterodyne near-field scattering,[9] and a form of schlieren interferometry.[10] All three of these methods are closely related and use a similar apparatus. A relatively large-diameter beam passes through a thin sample confined between plane-parallel windows and then falls on a pixilated sensor. Interference between the scattered light and the beam results in spatial- and time-dependent fluctuations in the local intensity. These fluctuations are measured by using a CCD or complementary metal-oxide semiconductor camera to digitize the transmitted beam intensity (or a portion of it) repeatedly. Spatial Fourier transformation of the intensity fluctuations allows one to obtain information about the scattered field for various scattering wave vectors. This is possible because light scattered at a given angle results in weak interference fringes of a given wavelength, and the different wavelengths may be separated by Fourier analysis. In practice, these methods rely on the fact that the fluctuations of interest are time dependent, while fluctuations resulting from stray elastically scattered light are time independent. Thus taking a sequence of images and analyzing differences or ratios of images allows one to quantify the small time-dependent fraction of the fluctuations. Of course, the fluctuations must be slow enough and large enough in amplitude to produce intensity modulations than can be accurately captured. These methods have the advantage of being nearly immune to the effect of stray elastically scattered light, such as that originating from optical surfaces, provided that such stray light is weak compared with the transmitted beam and remains constant in time.

Of course, it is sometimes possible to visualize a pattern of fluctuations directly, as is achieved for convection patterns[13,14] or electroconvection patterns by using a shadowgraph,[15] or, for example, by using a microscope to examine a liquid-crystal film between crossed polarizers.[16,17] In the later case the director fluctuations alter the polarization of the light transmitted by the liquid crystal locally, resulting in spatial- and time-dependent intensity fluctuations in the light emerging from the analyzing polarizer. In such cases one may decompose images into their spatial Fourier components and deduce their mean-squared amplitude and dynamic behavior; but we do not think such direct space-visualization methods should be considered scattering and do not discuss them further.

In considering the scattering (or, alternatively, diffraction) of light from the beam while it is passing through the sample, one should distinguish between two regimes. For sufficiently long wavelengths, a fluctuation of a given wave vector diffracts light from the beam coherently into both positive and negative orders, resulting in a coherent set of diffracted beams. In the diffraction of light by ultrasound,[18] this is referred to as the Raman–Nath regime. For sufficiently weak fluctuations, the diffraction is confined to the lowest order, and it is only under these conditions that a simple interpretation of the results seems possible. In this regime the technique could be called that of a quantitative shadowgraph,[12] and it was first used by Wu *et al.*[6] to measure the mean-squared amplitude of the temperature fluctuations in a horizontal layer of high-pressure gas below the onset of convection. In the shadowgraph regime a refractive index fluctuation having a given transverse wave vector acts as a weak phase grating and diffracts light coherently into a single positive order and a single negative order. These two diffracted beams are phase coherent with each other, and as they propagate beyond the sample they interfere with the transmitted beam to produce a fringe pattern having the same wave vector as that of the original fluctuation. The contrast of this fringe pattern is periodic in the product of the distance z from the sample and the squared wave vector q^2, which is a manifestation of the Talbot effect.[19] Because of this effect, the shadowgraph has an oscillatory transfer function[12] $T(q) = \sin^2 [q^2 z/(2k)]$, where k is the vacuum wave vector of the light. If the sample refractive index fluctuations are sufficiently weak, Fourier analysis of the interference pattern can be used to separate the contributions of the various wave-vector fluctuations[12] and thus determine the product of $T(q)$ and the static structure factor of the sample $S(q)$.

For sufficiently large wave vectors, ($q^2 \geq k\pi/d$, where d is the sample thickness), one enters the Bragg regime.[18] In this regime the scattering into positive and negative orders is incoherent, and the fringes generated by interference with the transmitted beam extend throughout the region of overlap between the scattered light and the beam. Consequently, the transfer function is q independent. Techniques operating in this regime have been pioneered by Giglio *et al.*, who named it near-field scattering[7–9] and used it to study scattering from colloids. They considered both the homodyne case,[7,8] in which the transmitted beam is removed and the speckles formed by the scattered light alone are measured, and the heterodyne case,[9] in which the speckles form because of interference between the transmitted beam and the scattered light. Their research has resulted in the interesting insight that in this regime the spatial correlation range of the speckle field reflects the size of the scattering particles rather than the intensity distribution of the source, as it does for speckles formed sufficiently far from the source. Basically, in the near-field scattering regime the size of the speckles corresponds directly to the size of the scattering particles.[7]

In an attempt to discover a method having a q-independent transfer function, even for wave vectors in the Raman–Nath regime, some of us[10] have developed a schlieren method. In this method light leaving the sample (including the transmitted beam) is brought to a focus, and an opaque blade is used to block the diffracted light corresponding to half the orders, resulting in a q-independent transfer function. The schlieren method involves an optical ar-

rangement very similar to that of a shadowgraph, but it utilizes spatial filtering to eliminate the oscillations in the transfer function. To understand how this is possible, recall that a sufficiently weak fluctuation of any particular wave vector results in two diffracted beams, one of which comes to a focus on one side of the focal spot corresponding to the main beam, while the other beam is focused exactly opposite to the first. Thus using an intensity mask, such as a razor blade, to block half the transmitted beam and all the light on one side of the beam removes half the diffracted light and produces interference fringes with a contrast independent of the visualization distance and the wave vector. The interference pattern resulting from scattering at a given wave vector then occurs between a single beam scattered at a small angle θ and the transmitted beam. This gives rise to a set of sinusoidal fringes with the same wavelength as the original sinusoidal phase modulation. Consequently, the schlieren transfer function is constant, and Fourier analysis of the images provides $S(q)$ directly, free of the shadowgraph transfer function, much like ordinary static light scattering.

Both the quantitative shadowgraph and the schlieren-based method have distinct advantages with respect to ordinary scattering techniques in that they are capable of operating at extremely small wave vectors (of the order of cm^{-1}), where stray-light problems make ordinary scattering methods useless. Moreover, these techniques allow for relatively rapid measurement of slow fluctuations because many statistically independent samples are acquired simultaneously at many different wave vectors. The main advantage of the schlieren method is the elimination of $T(q)$, but this advantage comes with a price. While the shadowgraph needs virtually no alignment at all and is extremely rugged, schlieren requires accurate positioning of the intensity mask and the use of high-quality optical elements, together with excellent mechanical stability, to attain a sharp, stable focusing of the beam. Even slight convective motion of air within the beam path can affect the correct pointing of the beam and impair the measurement. However these difficulties can be overcome, and both the schlieren method and the quantitative shadowgraph allow one to perform measurements in a wave-vector range not accessible with traditional small-angle light-scattering techniques.

In principle, all the methods outlined above can also be used to study dynamics and to obtain the same information provided by DLS. Dynamic measurements made by using a shadowgraph were reported by Rehberg *et al.*,[5] and we have been able to use both the shadowgraph and the schlieren methods to measure the autocorrelation function of the fluctuations for mixtures undergoing free diffusion. We have also been able to use the shadowgraph method to measure the temporal power spectrum of fluctuations in both a single-component fluid (CS_2) and a mixture (toluene and hexane) heated from above. Dynamic measurements have also been performed by using the near-field scattering technique to investigate the dynamics of diffusion in colloidal suspensions.

In this paper we report results showing that dynamic data may be obtained over a wide range of scattering wave vectors by using the schlieren method. We have applied this method to measure the autocorrelation function of fluctuations in a mixture of water and urea undergoing free diffusion. The results are similar to those obtained by us for free diffusion in a mixture of water and glycerol, via the shadowgraph method, which will be reported in a future publication. Both sets of results show that the correlation time reaches a maximum at a time-dependent crossover wave vector q_c and actually *decreases* with decreasing wave vector below q_c. In this paper we describe a method of processing the images to simultaneously provide both static and dynamic data. We have chosen to study gradient-driven fluctuations in a free-diffusion process because it is convenient and has strong fluctuations at low wave vectors, but the method should have general validity.

C. Fluctuations during Free Diffusion

Free diffusion in the absence of convection occurs when a stabilizing concentration gradient is generated in an isothermal mixture of two miscible fluids. A simple way to prepare a free-diffusion experiment in the presence of a constant gravitational field is to layer the two fluids, with the denser below the lighter, to obtain an initially flat horizontal interface between the two. As time passes, the initially sharp interface slowly broadens owing to diffusion. It has been shown[11,20,21] that a free-diffusion process is always accompanied by the presence of nonequilibrium fluctuations. These fluctuations result in strong scattering of light from a beam that passes vertically through the sample, i.e., perpendicular to the original interface. The origin of the enhanced fluctuations is the coupling of thermal velocity fluctuations to concentration due to the presence of the concentration gradient. Physically, any fluid element that is displaced vertically creates a concentration fluctuation. This coupling creates large-amplitude long-wavelength concentration fluctuations that result in strong scattering. Detailed theoretical results for the behavior of fluctuations in the free-diffusion case are developed in Ref. 22, in which Landau's fluctuating hydrodynamics[23] as used by Segrè *et al.*[24,25] in the case of a stationary linear gradient is extended to nonequilibrium fluctuations in time-dependent diffusion processes.

The authors of Ref. 22 assume that the fluid properties do not vary significantly throughout the sample, and they make use of two basic assumptions to simplify the calculations. The first is $D/\nu \ll 1$, where D is the diffusion coefficient and ν is the kinematic viscosity. This approximation is very accurate for almost all mixtures. Second, it is assumed that $q \gg (4D/\nu)^{1/4} q_c$, with q_c being a crossover wave vector given by

$$q_c(t) = \left[\frac{\beta g \nabla c(t)}{\nu D}\right]^{1/4}, \quad (1)$$

where $\beta = (1/\rho)(d\rho/dc)$ is the solutal expansion coefficient, g is the gravitational acceleration, and $\nabla c(t)$ is the concentration gradient, which decreases with time. The second assumption does not always hold for our experiment, but deviations from the exact equations were checked to be less than 5%. For fluctuations having $q \ll q_c$, buoyancy forces play a large role in the dynamics, while diffusion dominates for $q \gg q_c$. Assuming that the altitude for which the maximum concentration gradient is achieved generates most of the scattered signal,[11,20–22] the static power spectrum of the fluctuations at time t after establishing the initial gradient is predicted to be

$$S(q, t) = \frac{S_0(t)}{1 + [q/q_c(t)]^4}. \quad (2)$$

The prefactor $S_0(t)$ is given by

$$S_0(t) = \frac{1}{(2\pi)^2} k_B T \left(\frac{\partial n}{\partial c}\right)^2 \frac{\Delta c(t)}{\rho \beta g}, \quad (3)$$

where k_B is Boltzmann's constant, T is the absolute temperature, n is the refractive index, ρ is the sample density, and $\Delta c(t)$ is the time-dependent concentration difference between the top and the bottom of the sample.

The static structure factor $S(q, t)$ is thus a power law of the form q^{-4} for wave vectors that are sufficiently larger than the crossover value q_c. For $q \ll q_c$, $S(q, t)$ is q independent and equal to $S_0(t)$. As the free-diffusion process continues, the crossover wave vector q_c decreases slowly with time owing to the steadily decreasing concentration gradient, while $S_0(t)$ remains nearly constant until the diffusing zone reaches the boundaries and $\Delta c(t)$ begins to decrease with time.[20,22]

The dynamic structure factor $S(q, \omega)$ is calculated under the same assumptions, and by Fourier transforming it we obtain the temporal correlation function $G(q, dt)$, which is a decaying exponential with a correlation time given by

$$\tau(q, t) = \frac{1}{Dq^2\{1 + [q_c(t)/q]^4\}}. \quad (4)$$

The time constant $\tau(q, t)$ is approximately $1/(Dq^2)$ for $q \gg q_c$, corresponding to the well-known diffusive decay of fluctuations. For $q \ll q_c$, the time constant is $q^2/(Dq_c{}^4) = [1/(Dq^2)](q/q_c)^4$, and the decay of fluctuations is much more rapid than would be expected for diffusive decay at the same wave vector. This is identified as a nondiffusive, gravitational, regime in which fluctuations are relaxed primarily by buoyancy effects. The maximum in $\tau(q, t)$ occurs for $q = q_c$; consequently, such fluctuations represent the most slowly relaxing mode in the system.

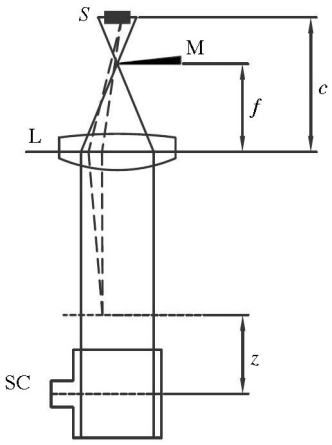

Fig. 1. Schematic diagram of the schlieren apparatus.

2. Experimental Methods and Results

A. Optical Setup

The optical setup of the schlieren apparatus we used is illustrated in Fig. 1. The output of a 10 mW He–Ne laser was spatially filtered and collimated to provide a plane-parallel beam with a $1/e^2$ diameter of ~20 mm.

The beam passed vertically upward through the sample cell SC, and was brought to a focus by lens L, (a 50 mm diameter achromatic doublet with a focal length $f = 100$ mm). An intensity mask M, placed a distance f from the lens blocked all light lying in one half of the Fourier plane. The sensor was placed at a distance of $c = 194$ mm beyond the lens, with c chosen so that light coming from a square portion of the cell of side $W \cong 0.45$ cm fell onto the sensor, which is a square array of 512×512 pixels . The cell has an inner diameter of 20 mm, and the parallel windows are separated by 20 mm.

With this arrangement, the intensity distribution in a plane at a distance z from the sample was imaged onto the sensor. The value of the distance z was of the order of a couple of centimeters, a visualization distance for which the shadowgraph would produce an extremely small signal owing to the zero in the transfer function at $z = 0$. However, the schlieren method eliminates this problem, and it can be used with virtually zero distance from the plane imaged onto the CCD and the sample, while the shadowgraph produces no signal under these conditions.

The size of the image digitized sets the minimum possible wave vector as $q_{\min} = 2\pi/W$, but using simple geometrical optics to calculate W, and thus the wave-vector calibration, is not very accurate. Instead, we placed a Ronchi ruling with 118 lines/cm (300 lines/in.) in the beam, located where the sample cell was normally positioned. This produced straight parallel interference fringes of an accurately known fundamental wave vector (742.1 cm^{-1}) on the sensor's surface. We acquired a set of 128 such images with different orientations of the grating. Spatial Fourier analysis of these images showed a strong peak at

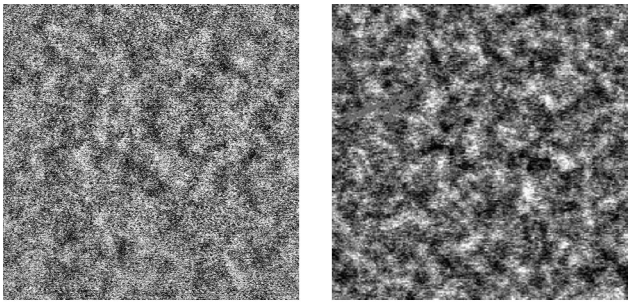

(a) (b)

Fig. 2. Difference images showing fluctuations for two different liquids undergoing free diffusion. (a) Schlieren image of a 4.5 mm square area showing fluctuations in a urea–water sample. (b) Shadowgraph image of a 4.5 mm square area showing fluctuations in a glycerol–water sample.

53.73 times the fundamental wave vector $q_{\min}$, as well as several harmonics. From this we obtained $q_{\min} = 13.81\ \mathrm{cm}^{-1}$, corresponding to $W = 0.455$ cm. In practice, we were limited to wave vectors of at least $3\ q_{\min}$ to acquire adequate statistical precision with the limited number of images processed. The maximum useful wave vector was set by the photon shot-noise level and was $\sim 1000\ \mathrm{cm}^{-1}$.

B. Experimental Procedure

The cell was first filled with water, and then the urea solution (44 wt. % in water) was injected from below. Both liquids were filtered and left at room temperature together with the cell for several hours before use. Enough solution was injected to bring the initial interface to about midheight of the cell. In this way the desired initial condition of a sharp macroscopic concentration gradient in a relatively isothermal sample was achieved. We roughly estimate that the initial temperature differences could have been as large as 0.2 °C, but we saw no evidence of convective flows.

Defining $t = 0$ as the time the filling procedure was completed, we took three sets of 128 images each, with the images separated in time by 0.080 s. These image sequences were initiated at times of 600, 1200, and 4200 s. The time delay Δt between images was chosen to allow significant correlation between successive images, and the total number of images was large enough to obtain the desired accuracy. Each image $I(\mathbf{x}, t)$ was divided by its average value to obtain the normalized intensity $i(\mathbf{x}, t) = I(\mathbf{x}, t)/\langle I(\mathbf{x}, t)\rangle_{\mathbf{x}}$. Difference images $\delta i(\mathbf{x}, t) = i(\mathbf{x}, t) - i_0(\mathbf{x})$ were then calculated to reveal the fluctuations. Here the optical background image $i_0(\mathbf{x})$ is the dimensionless intensity in the absence of the signal of interest, i.e., the beam profile. Experimentally, the background image was estimated separately for each sequence by averaging the 128 dimensionless intensities $i_0(\mathbf{x}) = \langle i(\mathbf{x}, t)\rangle_t$.

Figures 2(a) and 2(b) show typical images of nonequilibrium fluctuations obtained by means of the schlieren and shadowgraph techniques, respectively. Figure 2(a) is a difference image from the sequence initiated at $t = 4200$ s, and it has been scaled up by a factor of 60. Figure 2(b) shows a difference image obtained by using a shadowgraph to study a 40 wt. % glycerol sample diffusing into water, but with an amplification factor of 30. The schlieren image appears smoother than the shadowgraph one. Within the latter it is perhaps possible to recognize a typical size corresponding to the first maximum in the shadowgraph transfer function.

C. Image Processing

Data for each time studied were obtained by processing a single image sequence consisting of $128, 512 \times 512$, 8-bit schlieren images $I(\mathbf{x}, t)$, taken at equally spaced time intervals of $\Delta t = 0.080$ s. The dynamic processing procedure we used relies on statistical analysis of the time-dependent difference signal $\tilde{\delta i}(\mathbf{q}, t, \mathrm{d}t) = i(\mathbf{q}, t + \mathrm{d}t) - i(\mathbf{q}, t)$, obtained by subtracting normalized images $i(\mathbf{x}, t) = I(\mathbf{x}, t)/\langle I(\mathbf{x}, t)\rangle_{\mathbf{x}}$ taken with various time separations $\mathrm{d}t$. Here $i(\mathbf{q}, t)$ is the spatial Fourier transform of $i(\mathbf{x}, t)$. Using these difference images, we calculated the measured time-dependent structure function[26] $C_m(\mathbf{q}, \mathrm{d}t)$, which we define as

$$\begin{aligned} C_m(\mathbf{q},\ \mathrm{d}t) &\equiv \langle\, |\, \tilde{\delta i}(\mathbf{q},\ t,\ \mathrm{d}t)\, |^2\rangle_t \\ &= 2\langle\, \big|i(\mathbf{q},\ t)\big|^2\rangle_t - 2\ \mathrm{Re}\langle i(\mathbf{q},\ t) \\ &\quad \times\ i^*(\mathbf{q},\ t + \mathrm{d}t)\rangle_t, \end{aligned} \tag{5}$$

where the averaging with respect to time means over a single sequence of images. The time delay $\mathrm{d}t$ was varied from Δt to $64\ \Delta t$. Thus longer time delays involved averaging over fewer difference images, with the minimum delay involving averaging over 127 difference images and the largest delay over 63 images. The first term on the right-hand side of Eq. (5), $\langle |i(\mathbf{q}, t)|^2\rangle_t$, is related to the structure factor of the system by

$$\begin{aligned} \langle |i(\mathbf{q},\ t) - i_0(\mathbf{q})|^2\rangle_t &= AS(\mathbf{q}) + B(\mathbf{q}) \\ &= \langle |i(\mathbf{q},\ t)|^2\rangle_t - |i_0(\mathbf{q})|^2. \end{aligned} \tag{6}$$

Here A is a constant, and $i_0(\mathbf{q})$ is the Fourier transform of the beam profile, which we estimated for each sequence by averaging the images of that sequence. The quantity $B(\mathbf{q})$ is an electronic background that accounts for noise sources in the acquisition process, such as read noise, digitization effects, and shot noise. The second term on the right-hand side of Eq. (5), $\mathrm{Re}\langle i(\mathbf{q}, t) i^*(\mathbf{q}, t + \mathrm{d}t)\rangle_t$, is related to the temporal autocorrelation function of the fluctuations $G(\mathbf{q}, \mathrm{d}t)$ by

$$\begin{aligned} &\mathrm{Re}\langle [i(\mathbf{q},\ t) - i_0(\mathbf{q})][i^*(\mathbf{q},\ t + \mathrm{d}t) - i_0{}^*(\mathbf{q})]\rangle_t \\ &\quad = AS(\mathbf{q})G(\mathbf{q},\ \mathrm{d}t) \\ &\quad = \mathrm{Re}\langle i(\mathbf{q},\ t) i^*(\mathbf{q},\ t + \mathrm{d}t)\rangle_t - |i_0(\mathbf{q})|^2. \end{aligned} \tag{7}$$

Although each image includes a noise contribution, the noise is uncorrelated from image to image and thus does not appear in Eq. (7), which holds for $dt \neq 0$. Consequently, using Eqs. (5)–(7), the measured structure function $C_m(\mathbf{q}, dt)$ is related to the static power spectrum of the concentration fluctuations $S(\mathbf{q})$ and to their temporal autocorrelation function $G(\mathbf{q}, dt)$ by

$$C_m(\mathbf{q}, dt) = 2\{AS(\mathbf{q})[1 - G(\mathbf{q}, dt)] + B(\mathbf{q})\}. \quad (8)$$

The correlation function $G(\mathbf{q}, dt)$ is normalized so that it becomes unity when the delay time dt goes to zero, and it decreases to zero in the limit of infinite delay time. Of course, as diffusion proceeds, both $S(\mathbf{q})$ and $G(\mathbf{q}, dt)$ change with time, but in the interest of notational clarity we have not indicated this explicitly.

Because the system exhibits azimuthal symmetry, the results are dependent only upon the magnitude of the wave vector and not upon its direction. Thus we may average data for all wave vectors within a narrow range, which results in a statistical advantage that can be quite significant. This averaging process must be carried out after the processing; otherwise, no advantage is obtained. (The effect is much like having a large number of independent collection channels for a conventional light-scattering instrument.) In practice, we averaged over bands of width $q_{\min} \cong 14\ \mathrm{cm}^{-1}$.

Given a theoretical or numerical form for $G(\mathbf{q}, dt)$, one may fit the azimuthal average of Eq. (8) to the data for any given wave vector and thus experimentally determine three different quantities, $AS(q)$, $G(q, dt)$, and the noise background $B(q)$, where q denotes $|\mathbf{q}|$. It is perhaps worth mentioning that it is not essential to know the theoretical form for $G(\mathbf{q}, dt)$; one may use any convenient fitting function provided it conforms to the data. One should also note that the static power spectrum obtained in this way does not require an independent measurement in the absence of the signal to determine the noise background $B(q)$, which is normally necessary, because the background noise is obtained directly as one of the fitting parameters.

3. Results

Structure functions were computed for various q values and different time delays $dt = n\Delta t$, where n is an integer that we allowed to range from 1 to 64. The correlation function for nonequilibrium fluctuations is predicted to have the form

$$G(q, dt) = \exp\left[-\frac{dt}{\tau(q)}\right], \quad (9)$$

and thus, taking the azimuthal average of Eq. (8), the structure function can be written as

$$C_m(q, dt) = 2\left(AS(q)\left\{1 - \exp\left[-\frac{dt}{\tau(q)}\right]\right\} + B(q)\right). \quad (10)$$

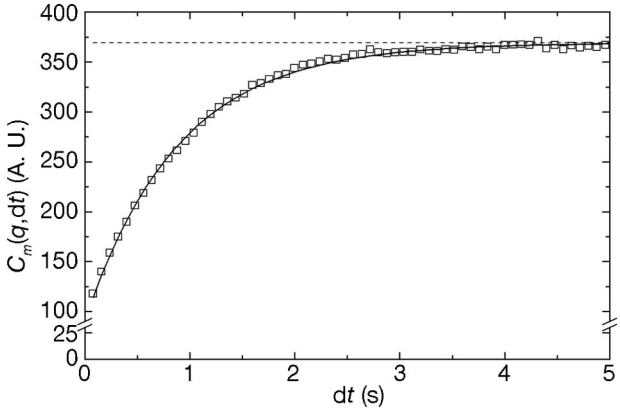

Fig. 3. Structure function $C_m(q, dt)$ measured at $t = 4200$ s as a function of time delay dt. The open squares are experimental data for $q = 277\ \mathrm{cm}^{-1}$, and the solid curve is the result of fitting Eq. (10) to the data. The dashed horizontal line is the fitted limit of $C_m(q, dt)$ for a long time delay.

Figure 3 shows a typical structure function measured at $t = 4200$ s for wave vector $q = 277\ \mathrm{cm}^{-1}$. The open squares are the experimental data points, and the solid curve is the result of fitting Eq. (10) to the data with $AS(q)$, $\tau(q)$, and $B(q)$ as adjustable parameters. The dashed horizontal line is the value $\lim_{dt\to\infty} C_m(\mathbf{q}, dt)$, which is twice the fitted value of $[AS(q) + B(q)]$. As the delay time approaches zero, the structure function (measured only for nonzero delays) has a well-defined limit equal to twice the background $B(q)$. Note that the structure function of the noise, which is uncorrelated from image to image, would show up only for a zero delay time and thus is not present in the data. The amplitude of the exponential decay is twice the static power spectrum $AS(q)$, while its time constant is the correlation time $\tau(q)$.

The constant schlieren transfer function allows one to make such measurements equally well for any wave vector in the accessible range, while for the shadowgraph such measurements are not practical for wave vectors near the zeros of the transfer function.

The first experimental result we obtain from fitting the structure functions at different q values is the static power spectrum of the nonequilibrium fluctuations (to within the multiplicative factor A, which we now drop). Figure 4 shows the results for the static structure factor determined at $t = 600$ and 4200 s. The solid curves are the results of fitting Eq. (3) to the data with S_0 and q_c as adjustable parameters. Data from $t = 1200$ s are not shown because they are almost identical to those for $t = 600$ s.

To make a direct comparison with results obtained by means of static analysis, we also obtained $S(q)$ directly from the same image sets by Fourier transforming the normalized difference images and then squaring and azimuthally averaging them to obtain $S(q) + B(q)$. We then obtained $B(q)$ by applying the same procedure to a set of 128 images acquired with

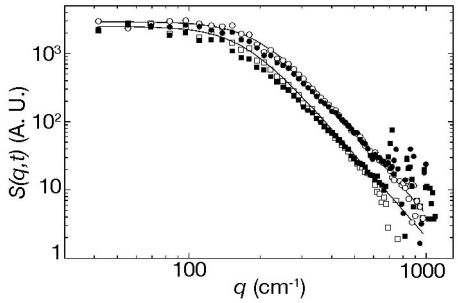

Fig. 4. Static structure factor $S(q, t)$ as a function of wave vector q as measured 600 s (open circles) and 4200 s (open squares) after establishing the interface. The solid curves fits of Eq. (3) to the data. The results of analyzing the same set of data images by using the static method are shown as solid symbols for comparison. For this analysis the background was determined separately, as described in the text.

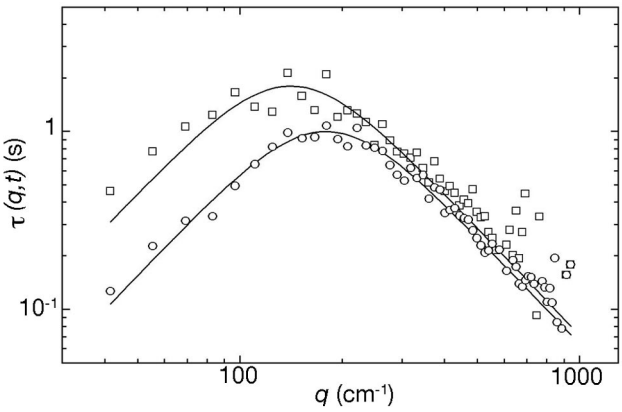

Fig. 5. Time constant $\tau(q, t)$ as a function of wave vector q for data taken 600 s (open circles) and 4200 s (open squares) after forming the interface. The solid curves are the results of fitting Eq. (4) to the data. As time increases, the crossover wave vector corresponding to the maximum value for τ decreases slowly, and the maximum time constant increases.

the sample cell totally filled with pure water, providing a direct measurement of $B(q)$. The results obtained for $S(q)$ in this more conventional way are shown in Fig. 4 as solid symbols. They have not been scaled in any way, and thus one can see that the two methods give very comparable results.

The transition from the q^{-4} decay above q_c to a constant amplitude in the buoyancy dominated region below q_c is clearly visible in the data, as well as a slight decrease of the crossover wave vector with time. Despite the fact that the extent to which diffusion has broadened the initial interface is rather different for the two times only a minor change in S_0 occurs, in agreement with Eq. (3), which indicates that this quantity depends on the concentration difference and not on the gradient. This result is very similar to those obtained previously by static analysis of either shadowgraph[11] or schlieren images.[10] However, unlike static analysis, the dynamic procedure outlined here does not require the separate measurement of background noise $B(q)$ and is thus more experimentally convenient.

The second result we obtain from fitting the structure function is the time constant $\tau(q, t)$. We can use these results to characterize the behavior of the dynamics of fluctuations for free diffusion. Figure 5 shows the results for $\tau(q, t)$ obtained for $t = 600$ and 4200 s. The solid curves are the results of fitting Eq. (4) to the data with D and q_c as adjustable parameters. Each curve has the expected shape in which a maximum in the time constant is clearly visible.

For wave vectors larger than q_c, τ is proportional to $1/(Dq^2)$ and the decay of fluctuations is diffusive, while for wave vectors smaller than q_c, it is proportional to $[1/(Dq^2)](q/q_c)^4$ owing to the effect of gravitational quenching. This gives rise to the intuitively strange result that longer-wavelength fluctuations relax more quickly than do shorter-wavelength ones in this regime. As the concentration profile evolves, the concentration gradient decreases, and the position of the maximum slowly shifts toward smaller q. At the same time, the dynamics at the smaller wave vectors become progressively slower. Fitting Eq. (4) to the data for $\tau(q, t)$ gives the diffusion coefficient $D \cong 1.12 \times 10^{-5}$ cm^2/s, which is consistent with the literature values.[27]

For comparison, we fit Eq. (2) to the data for $S(q)$, shown as open symbols in Fig. 4, to determine the static values for the crossover wave vector and used Eq. (4) to fit the data for $\tau(q, t)$ to obtain the dynamic values. The results are quite comparable, although the dynamic results are consistently somewhat smaller. The static data give crossover values of 193, 180, and 152 cm^{-1} for $t = 600$, 1200, and 4200 s, respectively, while the dynamic results for the same times are 179, 165, and 141 cm^{-1}, respectively.

4. Conclusions

We have described a dynamic light-scattering technique that relies on the processing of schlieren images. This technique allows one to measure both the static power spectrum and the temporal correlation function of a sample at extremely small wave vectors over a wave-vector range covering nearly two decades. Static data are equivalent to those obtained from static processing by using the schlieren technique[10] but without the need for a separate measurement of the background noise. Dynamic data appear to be equivalent to those obtained with dynamic shadowgraph, with the exception that the correlation functions obtained from shadowgraph images are noisy at those wave vectors where the sensitivity is small owing to the transfer function.

D. S. Cannell thanks NASA for support under grants NAG3-2439 and NNCO4GA45G.

References

1. See, for example, B. J. Berne and R. Pecora, *Dynamic Light Scattering with Applications to Chemistry, Biology and Physics* (Wiley, 1976), and references therein.
2. A. P. Y. Wong and P. Wiltzius, "Dynamic light scattering with a CCD camera," Rev. Sci. Instrum. **64,** 2547–2549 (1993).

3. L. Cipelletti and D. A. Weitz, "Ultralow-angle dynamic light scattering with a charge coupled device camera based multispeckle, multitau correlators," Rev. Sci. Instrum. **70,** 3214–3221 (1999).
4. F. Ferri, "Use of a charge coupled device camera for low-angle elastic light scattering," Rev. Sci. Instrum. **68,** 2265–2274 (1997).
5. I. Rehberg, S. Rasenat, M. de la Torre Juárez, W. Schöpf, F. Hörner, G. Ahlers, and H. R. Brand, "Thermally induced hydrodynamic fluctuations below the onset of electroconvection," Phys. Rev. Lett. **67,** 596–599 (1994).
6. M. Wu, G. Ahlers, and D. S. Cannell, "Thermally induced fluctuations below the onset of Rayleigh–Bénard convection," Phys. Rev. Lett. **75,** 1743–1746 (1995).
7. M. Giglio, M. Carpineti, and A. Vailati, "Space intensity correlations in the near field of the scattered light: a direct measurement of the density correlation function $g(r)$," Phys. Rev. Lett. **85,** 1416–1419 (2000).
8. M. Giglio, M. Carpineti, A. Vailati, and D. Brogioli, "Near-field intensity correlations of scattered light," Appl. Opt. **40,** 4036–4040 (2001).
9. D. Brogioli, A. Vailati, and M. Giglio, "Heterodyne near-field scattering," Appl. Phys. Lett. **81,** 4109–4111 (2002).
10. D. Brogioli, A. Vailati, and M. Giglio, "A schlieren method for ultra-low-angle light scattering measurements," Europhys. Lett. **63,** 220–225 (2003).
11. D. Brogioli, A. Vailati, and M. Giglio, "Universal behavior of nonequilibrium fluctuations in free diffusion processes," Phys. Rev. E **61,** R1–R4 (2000).
12. S. P. Trainoff and D. S. Cannell, "Physical optics treatment of the shadowgraph," Phys. Fluids **14,** 1340–1363 (2002).
13. S. W. Morris, E. Bodenschatz, D. S. Cannell, and G. Ahlers, "Spiral defect chaos in large aspect ratio Rayleigh–Benard convection," Phys. Rev. Lett. **71,** 2026–2029 (1993).
14. S. W. Morris, E. Bodenschatz, D. S. Cannell, and G. Ahlers, "The spatio-temporal structure of spiral-defect chaos," Physica D **97,** 164–179 (1996).
15. M. Denin, G. Ahlers, and D. S. Cannell, "Spatiotemporal chaos in electroconvection," Science **272,** 388–390 (1996).
16. Y. Galerne, I. Poinsot, and D. Schaegis, "Direct absolute measurements of the two-dimensional elastic constants in smectic C^* liquid crystal films," Appl. Phys. Lett. **71,** 222–224
(1997).
17. A. Yethiraj, R. Mukhopadhyay, and J. Bechoefer, "Two experimental tests of a fluctuation-induced first-order phase transition: intensity fluctuation microscopy at the nematic-smectic-A transition," Phys. Rev. E **65,** 021702-1-021702-16 (2002).
18. See, for example, M. V. Berry, *The Diffraction of Light by Ultrasound* (Academic, 1966).
19. H. F. Talbot, "Facts relating to optical science," Philos. Mag. **9,** 401 (1836).
20. A. Vailati and M. Giglio, "Giant fluctuations in a free diffusion process," Nature **390,** 262–265 (1977).
21. D. A. Weitz, "Diffusion in a different direction," Nature **390,** 233–235 (1997).
22. A. Vailati and M. Giglio, "Nonequilibrium fluctuations in time-dependent diffusion processes," Phys. Rev. E **58,** 4361–4371 (1998).
23. L. D. Landau and E. M. Lifshitz, *Fluid Mechanics* (Pergamon, 1959).
24. P. N. Segrè, R. Schmitz, and J. V. Sengers, "Fluctuations in inhomogeneous and nonequilibrium fluids under the influence of gravity," Physica A **195,** 31–52 (1993).
25. P. N. Segrè and J. V. Sengers, "Nonequilibrium fluctuations in liquid mixtures under the influence of gravity," Physica A **198,** 46–77 (1993).
26. E. O. Schulz-DuBois and I. Rehberg, "Structure function in lieu of correlation function," Appl. Phys. **24,** 323–329 (1981).
27. A. V. Wolf, M. G. Brown, and P. G. Prentiss, "Concentrative properties of aqueous solution: conversion tables," in *Handbook of Chemistry and Physics,* 69th ed. (CRC Press, 1988), pp. D264–D265.